Modeling of high-resolution $K\alpha$ emission spectra from Fe XVIII through Fe XXIV

V. Decaux,[1,2,*] V. L. Jacobs,[3] P. Beiersdorfer,[1] D. A. Liedahl,[1] and S. M. Kahn[4]
[1]*Department of Physics and Advanced Technologies, Lawrence Livermore National Laboratory, Livermore, California 94550, USA*
[2]*Space Sciences Laboratory, University of California, Berkeley, California 94720, USA*
[3]*Center for Computational Materials Science, Materials Science and Technology Division, Naval Research Laboratory, Washington, DC 20375-5000, USA*
[4]*Columbia Astrophysics Laboratory, Columbia University, New York, New York 10027, USA*
(Received 17 June 2002; published 30 July 2003)

Results for $K\alpha$ x-ray emission from highly charged iron ions, which were obtained from a detailed and systematic spectral model, are presented in the wavelength range from 1.84 to 1.94 Å. Account has been taken of the fundamental atomic radiative-emission processes associated with inner-shell electron collisional excitation, inner-shell electron collisional ionization, as well as dielectronic recombination. Particular emphasis has been directed at the identification of spectral features that can serve as diagnostics of extreme nonequilibrium or transient-ionization conditions, which can occur in stellar flares and supernova remnants, as well as in tokamak plasmas. In order to investigate the fundamental $K\alpha$ line-formation processes that can play a dominant role under these conditions, theoretical predictions have been compared with spectral observations of the EBIT-II x-ray emission from highly charged Fe ions in the electron-beam ion trap at the Lawrence Livermore National Laboratory. The observed spectroscopic features are found to be well represented by our theoretical calculations, validating earlier theoretical work on transient-ionization phenomena. We have identified spectral features that can serve as diagnostics of the electron density, the line-formation mechanism, and the charge-state distribution.

DOI: 10.1103/PhysRevA.68.012509 PACS number(s): 32.30.Rj, 32.70.Fw, 52.72.+v

I. INTRODUCTION

Due to the low electron density and near-equilibrium electron-energy distribution in solar and tokamak plasmas, the charge-state populations of the constituent ions can usually be determined within the framework of the standard steady-state coronal model. However, it has been demonstrated that unusual ionization conditions can occur when the emitting plasma is far removed from equilibrium. Nonequilibrium ionization conditions can prevail in the shock-front-heated regions of young supernova remnants [1–3] or in the impulsively heated gases in solar flares [4–9]. In these plasmas, the charge-state distribution can depart significantly from the standard corona-model distribution corresponding to the local electron temperature [7]. The x-ray emission can then occur from a much broader charge-state distribution, with appreciable components from many more charge states corresponding to the given element.

Laboratory electron-ion beam investigations, which have been performed using electron-beam ion traps developed at the Lawrence Livermore National Laboratory (LLNL), have led to significant advancements in the understanding of fundamental atomic processes in astrophysical and laboratory plasmas, particularly ionizing plasmas [10]. In order to provide a precise investigation of ionizing-plasma environments, a spectral simulation has been carried out using the EBIT-II electron-beam ion trap device at the LLNL. In this experiment, the $K\alpha$ x-ray emission spectra from iron ions were recorded under extreme transient-ionization conditions [11]. By means of the laboratory studies employing EBIT-II, it has been demonstrated that $K\alpha$ emission spectra can be used to reliably diagnose transient-ionization regions occurring in cosmic sources, and to identify young supernova remnants [12]. From a more refined analysis of the spectral data associated with the charge states Fe XVIII–Fe XXIV, it has been possible to deduce the ionization-time parameter $\eta = N_e t$, where N_e is the electron density and t is the time measured from the beginning of the ionizing process. This parameter has been considered to be a key quantity for the characterization of ionizing plasmas [13].

In this paper, we present a detailed and systematic theoretical model for the $K\alpha$ x-ray emission spectra from highly charged iron ions. In order to provide an accurate description for transient-ionization conditions, it has been necessary to extend a previously reported $K\alpha$ spectral model [14]. The revised atomic spectral model [15] is described in Sec. II. Particular attention has been given to the effects on the various line-formation processes of electron-density variations (as manifested by collisionally induced transitions competing with radiative-decay processes) and extreme nonequilibrium or transient-ionization conditions. A central result of our investigation is a systematic identification of the spectral features that can be used for the reliable diagnostics of the electron density and transient ionization.

II. THEORY OF LINE FORMATION IN TRANSIENT-IONIZATION PLASMAS

The total $K\alpha$ radiative-emission spectra can be generally represented as a superposition of the spectral intensities produced by the arrays of individual fine-structure transitions $j \rightarrow k$ in all abundant ions $Fe^{+(z)}$. Taking into account the

*Present address: Surface Integrity Group, Novellus Systems, 4000 N. First Street, MS/30-1A San Jose, California 95134.

electron-ion collision processes leading to *K*-shell excitation, radiationless (dielectronic) capture, and *K*-shell ionization, the total spectral intensity for a given incident electron energy ε_i may be expressed in the form

$$I(h\nu)=N_e\sum_z\sum_j\sum_k B_r(z,j\rightarrow k)L(z,j\rightarrow k,h\nu)\times[N(z)C_{\rm exc}(z,i',\varepsilon_{i'}\rightarrow j)+N(z+1)\times C_{\rm cap}(z+1,i,\varepsilon_i\rightarrow j)+N(z-1)\times C_{\rm ion}(z-1,i'',\varepsilon_{i''}\rightarrow j)]. \quad (1)$$

In this expression, which provides a generalization of our previously developed $K\alpha$ spectral model [14], the population densities of the initial Fe ions in the charge states $z+1$, z, and $z-1$ are denoted by $N(z+1)$, $N(z)$, and $N(z-1)$, respectively. The initial-ion quantum states in these three adjacent states of ionization are denoted, respectively, by i, i', and i''. N_e is the electron density. The individual rate coefficients C describing electron-impact excitation, radiationless electron capture, and electron-impact ionization are distinguished by means of the subscripts ''exc,'' ''cap,'' and ''ion,'' respectively. In our investigation, the quantum states involved in the spontaneous radiative transitions $j\rightarrow k$ in $Fe^{+(z)}$ are specific fine-structure states, which are specified by the total electronic angular-momentum quantum numbers J_j and J_k (hyperfine structure has been ignored in our investigation). The radiative-transition branching ratios $B_r(z,j\rightarrow k)$ are expressed by

$$B_r(z,j\rightarrow k)=\frac{A_r(z,j\rightarrow k)}{\sum_i A_a(z,j\rightarrow i,\varepsilon_i)+\sum_{k'} A_r(z,j\rightarrow k')}, \quad (2)$$

where $A_a(z,j\rightarrow i,\varepsilon_i)$ and $A_r(z,j\rightarrow k)$ denote the autoionization and the Einstein spontaneous radiative-transition rates, respectively. The quantities $L(z,j\rightarrow k,h\nu)$ are the frequency-normalized line-shape functions, allowing for Doppler broadening and natural broadening (due to autoionization and spontaneous radiative decay) in the isolated-resonance approximation. In order to take into account collisional and Stark broadenings, which are expected to play a dominant role at very high densities, a more general line-shape theory must be employed. In our experimental investigation, the distribution of incident electron energies is substantially wider than the spectral linewidths. Consequently, a detailed knowledge of the line-shape functions is not necessary.

For a general single-electron velocity distribution function $f_e(\vec{\nu}_e)$, the rate coefficients C for the three fundamental binary electron-ion collision processes may be related to the corresponding differential collision cross sections σ as follows:

$$C_{\rm exc}(z,i',\varepsilon_{i'}\rightarrow j)=\int\int d^3\nu_e d\Omega|\vec{\nu}_e|f_e(\vec{\nu}_e)\times\sigma_{\rm exc}(z,i',\varepsilon_{i'}\rightarrow j;\vec{\nu}_e,\Omega),$$

$$C_{\rm cap}(z+1,i,\varepsilon_i\rightarrow j)=\int\int d^3\nu_e d\Omega|\vec{\nu}_e|f_e(\vec{\nu}_e)\times\sigma_{\rm cap}(z+1,i,\varepsilon_i\rightarrow j;\vec{\nu}_e,\Omega),$$

$$C_{\rm ion}(z-1,i'',\varepsilon_{i''}\rightarrow j)=\int\int d^3\nu_e d\Omega|\vec{\nu}_e|f_e(\vec{\nu}_e)\times\sigma_{\rm ion}(z-1,i'',\varepsilon_{i''}\rightarrow j;\vec{\nu}_e,\Omega). \quad (3)$$

In these relationships, averages have been performed over the initial electron velocities $\overline{\nu_e}$ and integrations have been carried out over the angles Ω referring to the final scattered electron. (Integrations over the energy and angles of the ejected electron are also assumed to have been carried out in the definition of the electron-impact-ionization cross section.)

In most astrophysical and tokamak environments, equilibrium-plasma conditions are assumed to prevail. Accordingly, the electron-velocity (energy) distribution function $f_e(\vec{\nu}_e)$ is usually taken to be a Maxwellian. In our electron-beam ion trap (EBIT) investigation, however, the electron distribution is nearly monoenergetic and therefore can be adequately represented in the form

$$f_e(\vec{\nu}_e)=\delta^3\left(\vec{\nu}_e-\left(\frac{\varepsilon_{i'}}{E_H}\right)^{1/2}(\alpha c)\hat{z}\right), \quad (4)$$

where E_H is the hydrogen ionization energy, α is the fine-structure constant, and c is the velocity of light. In our EBIT experiment, the electron-beam energy is centered at 12 keV, for which we obtain $|v_e|=6.5\times10^9$ cm s^{-1}.

Assuming low-density conditions and ignoring charge-exchange processes, the dynamic (time-dependent) balance between the electron-ion ionization and recombination processes can be described by the set of coupled partial-differential equations:

$$\frac{\partial N(z)}{\partial t}+\vec{\nabla}\cdot[\vec{V}(z)N(z)]=N_eN(z-1)S_{\rm ion}(z-1\rightarrow z)-N_eN(z)S_{\rm ion}(z\rightarrow z+1)+N_eN(z+1)\alpha_{\rm rec}(z+1\rightarrow z)-N_eN(z)\alpha_{\rm rec}(z\rightarrow z-1). \quad (5)$$

The total ionization rate coefficient $S_{\rm ion}$ allows for both the elementary direct-ionization (di) process and the two-step process of autoionization (a) following inner-shell-electron excitation (ex):

$$S_{\rm ion}(z\rightarrow z+1)=\sum_j\left[S_{\rm di}(g\rightarrow j)+\sum_a C_{\rm ex}(g\rightarrow a)Q^{-1}(a,a)A_a(a\rightarrow j)\right]. \quad (6)$$

The total electron-ion photorecombination rate coefficient $\alpha_{\rm rec}$ allows for both the direct elementary radiative-

recombination (rr) process and the two-step process of (stabilizing) radiative decay (r) following radiationless electron capture (cap) into autoionizing resonances (corresponding to dielectronic recombination):

$$\alpha_{\rm rec}(z+1\rightarrow z)=\sum_b \left[\alpha_{\rm rr}(i\rightarrow b) + \sum_a C_{\rm cap}(i\rightarrow a)Q^{-1}(a,a)A_r(a\rightarrow b)\right]. \quad (7)$$

The quantities $Q(a, a)$ denote the diagonal elements of the matrix of the autoionization, collisional-transition, and radiative-transition rates. The nondiagonal elements of the matrix Q must be used in a more general (collisional-radiative model) calculation for the population densities of the autoionizing levels. In the corona-model approximation, which is valid at sufficiently low plasma densities, it is assumed that all recombining ions are initially in their ground states ($i=g$) and that all excited levels of the atomic system are depopulated only by means of autoionization or spontaneous radiative-emission processes. In this case, the quantity $Q(a, a)$ corresponds to the inverse of the total (natural) lifetime of the autoionizing resonance a and can be expressed as the sum of all permissible autoionization rates (A_a) and all allowed spontaneous radiative-decay rates (A_r):

$$Q(a,a)=\sum_i A_a(z,a\rightarrow i,\varepsilon_i)+\sum_b A_r(z,a\rightarrow b). \quad (8)$$

It should be pointed out that the class of autoionizing resonances that can participate in the indirect (two-step) dielectronic-recombination process is usually distinct from the class of autoionizing resonances that can be involved in the indirect- (two-step) ionization process of autoionization following inner-shell-electron excitation.

For equilibrium (Maxwellian) electron-velocity distributions, the electron-ion ionization and recombination rate coefficients $S_{\rm ion}$ and $\alpha_{\rm rec}$ are obtained as functions of the electron temperature T_e. Neglecting transport processes and time-dependent phenomena, the charge-state distributions $N(z)$ can be determined, as functions of the electron temperature, by means of the simple steady-state corona-model relations:

$$N(z)S_{\rm ion}(z\rightarrow z+1)=N(z+1)\alpha_{\rm rec}(z+1-z). \quad (9)$$

This approximation is often employed for stellar flares and tokamak plasmas.

It is widely recognized that the standard steady-state corona-model approximation does not provide a valid representation for an extreme nonequilibrium (transient-ionization) charge-state distribution, such as that produced in our present investigation using an electron-beam ion trap. In this case, it has been necessary to employ a time-dependent model for the determination of the relative ionic charge-state population fractions. An alternative method for the determination of the charge-state fractions is based on an analysis of the relative intensities of individual spectral-line features [16].

A formidable effort would be required for a detailed and precise calculation of the electron-impact (collisional) excitation cross sections for the multitude of fine-structure transitions involved in our spectral simulation. In order to provide a practical procedure for obtaining realistic values of the cross sections describing the numerous electron-impact excitation processes, which are needed to evaluate the first term in Eq. (1), we have employed the Born and Bethe (long-range dipole) approximations. Collisional excitation can occur for all values of the incident electron energy that are above the K-shell excitation threshold, which is about 6.4 keV for iron. For low-density plasmas, in which all ions can be assumed to be confined to their ground-electronic states, the product of the electron-impact excitation cross section and the incident electron velocity can be estimated by using the result [14]

$$\nu_e\sigma_{\rm exc}(z,i',\varepsilon_{i'}\rightarrow j)=\left(\frac{\varepsilon_{i'}}{E_H}\right)^{1/2}(\alpha c)\left(\frac{4\pi a_0^2}{\alpha^3}\right)\left(\frac{E_H}{\varepsilon_{i'}}\right) \times\left(\frac{E_H}{E_{ji'}}\right)^3 \ell n\left(\frac{4\varepsilon_{i'}}{E_{ji'}}\right) \times\left[\frac{g(j)}{g(i')}\right]\sum_{i'}\left(\frac{\hbar}{E_H}\right)A_r(z,j\rightarrow i'). \quad (10)$$

Here a_0 is the Bohr radius and $\hbar$ is Planck's constant divided by 2π. We have denoted by $E_{ji'}$ the excitation energy, which is equal to the photon energy that is emitted in the spontaneous $K\alpha$ radiative transition $j\rightarrow i'$. The factors $g(j)$ and $g(i')$ are used to denote the statistical weights of the excited-state and ground-state fine-structure levels, which are given by $2J_j+1$ and $2J_{i'}+1$, respectively. Note that the product of the excitation cross section and the incident electron velocity is expressed in the units of $c(a_0)^2$ or $\rm cm^3\,s^{-1}$, since $(\hbar/E_H)$ has the units of seconds, $A_r(z,j\rightarrow i')$ is measured in units of $\rm s^{-1}$, and the various energies have been expressed in a dimensionless form. The same units are conventionally adopted for the collisional-excitation rate coefficient due to plasma electrons. This simple formula is expected to overestimate the electron-impact excitation cross sections by a factor of 2 or 3 for incident electron energies very close to the excitation threshold values $E_{ji'}$. In order to compensate for this inadequacy, the correction factor of 0.5 recommended by Seaton [17] has been adopted in our calculations. In a future extension of this investigation, it would be desirable to employ more sophisticated (and possibly more realistic) calculations for the electron-impact excitation cross sections, such as those based on the distorted-wave or close-coupling approximations.

In a rapidly ionizing plasma, for which the inner-shell collisional excitation and (especially) the ionization mechanisms play the dominant role in the formation of the $K\alpha$ radiative emission, the process of radiationless electron cap-

ture is expected to be less important. Furthermore, since the electron-beam energy in our electron-beam ion trap experiment has been selected to be outside of the region of the autoionizing resonances, the dielectronic-recombination mechanism is not expected to provide any contribution in the formation of the $K\alpha$ spectra observed on EBIT-II. Accordingly, we can omit the second term in Eq. (1), which involves the radiationless electron-capture (inverse-autoionization) rate coefficient $C_{\rm cap}$.

The only remaining process (in addition to inner-shell collisional excitation) that can provide a significant contribution to the total $K\alpha$ spectral intensity is *K*-shell ionization by electron impact. This line-formation mechanism is described by the third term in Eq. (1). The electron-impact-ionization rate coefficient $C_{\rm ion}(z-1,i'',\varepsilon_i''\rightarrow j)$, which is defined in terms of an integration over the angles of the ejected electron, can be expressed in terms of summations over the total angular-momentum quantum numbers representing the ejected-electron residual-ion system. In the Born approximation, the ionization cross section can be expressed, in the LS-coupling representation, in terms of summations over the allowed values of the total angular-momentum quantum numbers *L*, *S*, and *J*. If a central-field picture is adopted for the determination of the electronic eigenstates, the ionization cross section connecting the pair of specific fine-structure states i'' and j can be simply reduced to the cross section for the ionization of a single electron from the active initial subshell $n_{i''}j_{i''}$. For more than one electron in the initial subshell, a factor of $N_{i''}$ should be included; and for a complex atomic structure it may be necessary to include a coefficient of fractional parentage. In our calculations, we have adopted the *K*-shell ionization cross sections of Lotz [18], allowing for a factor of ''2'' in order to take into account the number of electrons in the initial *K* shell. Unlike the situation for electron-impact excitation, we do not know of any readily available more-sophisticated methods that would provide guaranteed improvements with respect to the ionization cross sections of Lotz [18]. It should be pointed out that, for incident electron energies sufficiently high to produce *K*-shell ionization (8.68 keV for iron), it will also be necessary to consider additional line-formation processes involving cascade transitions from higher-lying excited electronic states.

In many astrophysical environments for which ionizing plasmas are encountered, such as supernova remnants, the electron density is sufficiently low so that all excited ionic-level populations in Eq. (1) can be assumed to be negligible in comparison with the ground-state population. Consequently, it is necessary to consider only the populations of the ground-electronic fine-structure states. This assumption had been expected to be valid for our measurements on EBIT-II as well as for stellar-flare plasmas, for which the electron density is characteristically in the range $10^{10}-10^{13}$ cm^{-3}. However, the results of our detailed spectral observations using EBIT-II have been found to be more accurately described in terms of an intermediate-density regime. In this intermediate-density regime, collisional processes are expected to redistribute an appreciable fraction of the population of the initial ions among excited fine-structure levels in a narrow energy range just above the ground fine-structure level. Accordingly, in the remainder of this paper, our theoretical spectral model will be applied to two distinct characteristic density regimes. The first is a low-density regime, for which the ionic-level population is assumed to be confined to the lowest-lying fine-structure level of the ground-state electronic configuration. The second is an intermediate-density regime, for which all fine-structure levels of the ground-state electronic configuration are assumed to be populated according to their statistical weights $2J+1$ but no levels of an excited electronic configuration are assumed to be populated. In an earlier version of our spectral model [14], results were also presented for a (third) high-density regime. In this high-density regime, statistical populations were assumed to be established for all fine-structure states of not only the ground-state electronic configuration but also for the low-lying optically excited electronic configurations. For the intermediate-density regime of interest in the present investigation, the term $g(i')$ in Eq. (10) should be replaced by a summation over all the lower levels i' that are assumed to be populated.

Only the populations of the charge states from Fe XVIII through Fe XXII are expected to be appreciably altered by the electron-density-sensitive electron-ion collisional-redistribution processes. This density sensitivity can be understood from the observation that, above some relatively low value of the electron density, the rates for the relevant collisionally induced transitions among the $2p$-subshell fine-structure states are characteristically much faster than the corresponding spontaneous radiative-transition rates. These spontaneous radiative transitions, which are forbidden by the electric-dipole angular-momentum and parity selection rules, have very slow rates. For the five charge states Fe XVIII–Fe XXII, the fine-structure levels of the ground-electronic configurations are as follows, starting from the ground fine-structure state (1) followed by the excited fine-structure levels (2) and (5) occurring above the ground fine-structure state (1):

Fe XVIII (F)	(1)	$1s^2_{1/2}2s^2_{1/2}2p^2_{1/2}2p^3_{3/2}\ ^2P_{3/2}$
	(2)	$1s^2_{1/2}2s^2_{1/2}2p_{1/2}2p^4_{3/2}\ ^2P_{1/2}$
Fe XIX (O)	(1)	$1s^2_{1/2}2s^2_{1/2}2p^2_{1/2}2p^2_{3/2}\ ^3P_2$
	(2)	$1s^2_{1/2}2s^2_{1/2}2p^2_{1/2}2p^2_{3/2}\ ^3P_0$
	(3)	$1s^2_{1/2}2s^2_{1/2}2p_{1/2}2p^3_{3/2}\ ^3P_1$
	(4)	$1s^2_{1/2}2s^2_{1/2}2p_{1/2}2p^3_{3/2}\ ^1D_2$
	(5)	$1s^2_{1/2}2s^2_{1/2}2p^4_{3/2}\ ^1D_2$
Fe XX (N)	(1)	$1s^2_{1/2}2s^2_{1/2}2p^2_{1/2}2p_{3/2}\ ^4S_{3/2}$
	(2)	$1s^2_{1/2}2s^2_{1/2}2p_{1/2}2p^2_{3/2}\ ^2D_{3/2}$
	(3)	$1s^2_{1/2}2s^2_{1/2}2p_{1/2}2p^2_{3/2}\ ^2D_{5/2}$
	(4)	$1s^2_{1/2}2s^2_{1/2}2p_{1/2}2p^2_{3/2}\ ^2P_{1/2}$
	(5)	$1s^2_{1/2}2s^2_{1/2}2p^3_{3/2}\ ^2P_{3/2}$
Fe XXI (C)	(1)	$1s^2_{1/2}2s^2_{1/2}2p^2_{1/2}\ ^3P_0$
	(2)	$1s^2_{1/2}2s^2_{1/2}2p_{1/2}2p_{3/2}\ ^3P_1$
	(3)	$1s^2_{1/2}2s^2_{1/2}2p_{1/2}2p_{3/2}\ ^3P_2$
	(4)	$1s^2_{1/2}2s^2_{1/2}2p^2_{3/2}\ ^1D_2$
	(5)	$1s^2_{1/2}2s^2_{1/2}2p^2_{3/2}\ ^1S_0$
Fe XXII (B)	(1)	$1s^2_{1/2}2s^2_{1/2}2p_{1/2}\ ^2P_{1/2}$
	(2)	$1s^2_{1/2}2s^2_{1/2}2p_{3/2}\ ^2P_{3/2}$

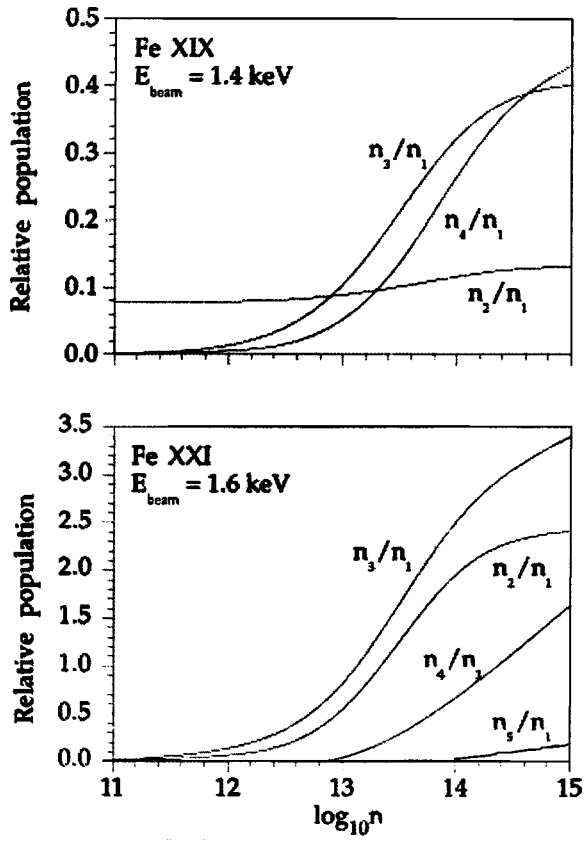

FIG. 1. Relative populations of the first four ground-state-configuration fine-structure levels as functions of the electron density n for (a) Fe XXI and (b) Fe XIX. The electron-energy distribution has been taken to be a Maxwellian equilibrium distribution corresponding to an electron temperature, centered at 1.6 keV for Fe XXI and at 1.4 keV for Fe XIX.

The capital letters in parentheses are used to indicate the fluorinelike, oxygenlike, nitrogenlike, carbonlike, and boronlike ions, respectively.

Figure 1 shows, for the ions Fe XIX and Fe XXI, the relative populations (n_j/n_1) of the individual excited fine-structure levels j of the ground-electronic-state configurations as functions of electron density (within the range from 10^{11} to 10^{15} cm^{-3}). These level populations have been determined from a separate collisional-radiative-model calculation using the Hebrew University Lawrence Livermore Laboratory Atomic Code (HULLAC) [19], with collisional rate coefficients computed assuming Maxwellian electron-energy distributions. Since the EBIT-II experimental results were obtained using a highly nonequilibrium electron-energy distribution, the results in Fig. 1 should be understood as providing only a qualitative representation of the relative populations pertaining to our electron-beam measurements. These two charge states are the only ones for which electron-ion collisionally induced mixing of the ground-electronic-configuration fine-structure states is found to be significant at electron densities equal to or less than 10^{12} cm^{-3}. Figure 1 provides confirmation that the ground-electronic-configuration fine-structure states j have relative populations n_j that are continuous functions of the electron density. However, the two characteristic electron-density regimes considered (low and intermediate) can be expected to provide only approximate representations for the determination of the level-population kinetics. For Fe XIX, the ratio n_2/n_1 remains essentially constant, at about 0.1, even at lower electron densities. This behavior may be attributable to the relatively weak collisionally induced redistribution of the populations for atomic states that differ only in the quantum numbers corresponding to the total electronic angular momentum J. A more significant degree of collisionally induced redistribution is found to occur for Fe XXI. For this ion, the populations of the levels 2 and 3 (which correspond to the fine-structure excitation of a $2p_{1/2}$ electron to the $2p_{3/2}$ level) account, respectively, for about 10% and 15% of the populations of the ground state 1 at $N_e = 10^{12}$ cm^{-3}. This collisional redistribution will be shown to have important consequences in the determination of the spectral-line intensities for the carbonlike complex. Our experimental data will also be compared with the theoretical results obtained by Lemen *et al.* [20]. These earlier theoretical results have been obtained from a more detailed collisional-radiative model, in which the electrons were assumed to be represented by a Maxwellian energy distribution. This more detailed model of Lemen *et al.* [20] provides a more refined treatment of the electron-density-dependent collisional redistribution of the level populations, but it has been applied only for the collisional-excitation contribution to the $K\alpha$ spectral intensities due to a Maxwellian electron-energy distribution. The predictions of this more detailed collisional-radiative model are found to be in better agreement with our experimental data in an intermediate-density regime, corresponding to a value for N_e of 10^{13} cm^{-3}. However, this comparison should not be taken as ideal, because our experimental data reflect the excitation spectra due to a highly nonequilibrium electron-energy distribution.

III. LABORATORY SIMULATION OF TRANSIENT-IONIZATION PLASMA CONDITIONS

Transient conditions, which are necessary for the observation of the lower charge states of iron, have been achieved in the laboratory using the LLNL EBIT-II electron-beam ion trap [21,22]. In EBIT-II, an electron beam is produced by a Pierce-type electron gun and compressed to a radius of $\sim$30 μm by a 3 T magnetic field, which is generated by a pair of superconducting Helmholtz coils. The space-charge field of the electron beam confines the ions, and collisions with beam electrons produce ionization from the trapped ions and excitation of the inner-shell-electron x-ray transitions. Individual ion orbits correspond to motion into and out of the electron beam and, therefore, to the influence of different regions of electron density. Accordingly, the ions are collectively exposed to an average electron density that can be substantially (two to five times) lower than the characteristic electron density that is determined by the radius, energy, and current of the electron beam. By tuning the nearly monoenergetic electron beam (which has an energy spread $\approx$50 eV full width at half maximum), it is possible to select a particular excitation mechanism in a given ion. Because the emitting ions are

nearly stationary, the observed x-ray lines have negligible Doppler shifts. Consequently, the electron-beam ion trap is an ideal device for high-precision spectroscopy. Since this device was originally designed as an x-ray source, six radial ports allow viewing of the trapped ions in a plane perpendicular to the electron beam. The measurements presented in this paper were carried out using a high-resolution crystal spectrometer in the von Hámos configuration [23,24]. In these experiments, the conditions on EBIT-II were the following: beam current $I_{\mathrm{beam}}=150$ mA, ion density $N_i \approx 10^9$ cm^{-3}, and current density $J \approx 5300$ Å cm^{-2}.

As noted above, the characteristic excitation energy of the $K\alpha$ transitions is significantly higher than the electron-beam energy required to produce an appreciable population of Fe ions corresponding to the intermediate charge states Fe XVIII–Fe XXIV. Because we employ a nearly monoenergetic electron beam with a relatively high energy, these intermediate charge states would be expected to have negligible populations under steady-state excitation conditions. Accordingly, we have developed a data-routing technique to simulate a nonequilibrium, transient-ionization process similar to that occurring in supernova remnants. Our procedure, which has been described by Decaux and Beiersdorfer [11], is as follows: first, singly or doubly charged iron ions produced by a metal vapor vacuum arc (MeVVA) [25] are injected into EBIT-II at a time $t=0$ s, initiating the interaction with the electron beam. MeVVA injection has the advantage that all material enters the trap at the beginning of the ionization process. The iron atoms do not enter the trap after the MeVVA firing. Although iron ions emerge from the trap in a continuous manner following an ion confinement on a time scale of several seconds, these ions are not recycled into the plasma as neutrals but instead adhere to the surfaces of the drift tubes. Then a series of 15 spectra are recorded sequentially during the ionization process. The time scale for the production of Fe XXV ions, and therefore for the observation of transient-ionization spectra, is less than 1 s. For the lower charge states below Fe XXI, this time scale is as short as a few milliseconds. After the 15 spectra have been recorded, the ions are removed from the trap. This process is repeated many times over a period of several hours. In addition, neutral N_2 is introduced into the trap using a ballistic gas injector system. This has a dual purpose: first, the injection of low-Z neutral gas in EBIT-II has been demonstrated to be an effective method for the attainment of longer trapping times for the high-Z ions of interest, using a process known as evaporative cooling [26]. Second, a charge-exchange process, which involves the interaction of iron ions with the neutral N_2 in the trap, corresponds to a recombination mechanism that impedes the rate for ionization. This allows additional time to record the x-ray emission from the lower charge states. However, charge exchange cannot produce *K*-shell line emission in the absence of bare or hydrogenlike iron ions, i.e., in the absence of iron ions with a *K*-shell vacancy. Since those charge states are not produced in the ionizing phase considered in our experiments, we can, therefore, neglect charge-exchange recombination in the modeling of the $K\alpha$ emission spectra. In order to provide an unambiguous simulation of the nonequilibrium, transient-ionization processes, we have selected the electron-beam energy to be outside of the region of the autoionizing resonances contributing to dielectronic recombination.

Due to the significantly different rates for the competing excitation processes, the laboratory observation of the $K\alpha$ radiative emission from the lower charge states presents an especially challenging problem. For electron energies relevant to the production of line emission from ionizing plasmas, the cross sections for collisional excitation and *K*-shell ionization are of the order of a few times 10^{-22} cm^2. However, the cross sections for *L*- and *M*-shell ionization processes, which do not lead to $K\alpha$ line formation, are 5×10^{-20} and $(0.44-1.1)\times 10^{-18}$ cm^2, respectively. As we will discuss in the following section, the cross sections for collisional excitation and *K*-shell ionization are of the same order of magnitude. This has provided the motivation for the collection of the majority of the spectral data, especially the data relevant to the lowest charge states below Fe XXII, at an electron-beam energy above the threshold for *K*-shell ionization (which is 8.68 keV for iron).

IV. COMPARISON OF THEORETICAL AND EXPERIMENTAL RESULTS

The experimental spectrum was obtained using a LiF(200) crystal bent to a radius of curvature R_c of 75 cm, with a spectral resolution $\lambda/\Delta\lambda \sim 2300$. The spectral data were recorded over a period of about 41 h with an electron-beam energy of 12 KeV, which is above the Fe *K*-shell ionization threshold. The data were calibrated with reference to the strongest of the two Fe XVIII lines ($F1$, $1s^2 2s^2 2p^5\ ^2P_{3/2}$-$1s 2s^2 2p^6\ ^2S_{1/2}$) and the most prominent Fe XXI feature ($C9$,$1s^2 2s^2 2p^2\ ^3P_0$-$1s 2s^2 2p^3\ ^3D_1$). For these two reference lines, the adopted wavelengths were 1.926 79 and 1.894 50 Å, respectively. These wavelengths were determined from earlier measurements. These two reference lines were chosen because of their high intensity and adequate separation. A reliable calibration of the dispersion is thereby obtained in the relevant wavelength range. The experimental error is of the order of 0.5 mÅ. Because of the extended period of time that is necessary to accumulate a sufficient intensity of the iron x-ray line emission, counts induced by cosmic rays and general electronic noise form an elevated background that must be discounted in the comparison of the experimental data with the results predicted by the theoretical models.

It is desirable to assess the validity of the theoretical predictions, especially for the lower (less-frequently investigated) charge states from Fe XVIII–Fe XXI. Accordingly, we present comparisons of the distinctive theoretical results predicted for dielectronic recombination, collisional excitation, and *K*-shell ionization, together with the experimental data obtained from EBIT-II in the wavelength range from 1.885 to 1.940 Å. The results shown in Fig. 2 exhibit the theoretically predicted contributions that would be observed from dielectronic recombination (if the electrons had been represented by a Maxwellian energy distribution) for (a) the low-density regime and (b) the intermediate-density regime. (A vanishing contribution for dielectronic recombination would be pre-

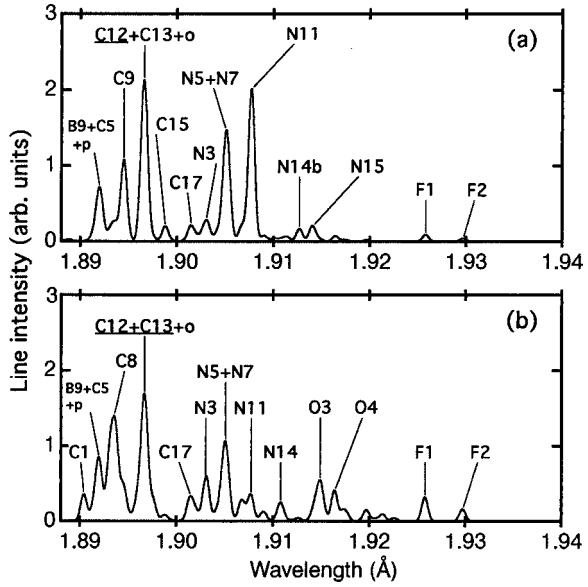

FIG. 2. Theoretically predicted spectra for the dielectronic-recombination contribution to the $K\alpha$ emission from Fe XVIII–Fe XXI, in the wavelength range 1.89–1.94 Å. The spectral results are presented for the low-density (a) and intermediate-density (b) regimes, which have been defined in Sec. II of the text as well as previously by Jacobs *et al.* [14]. The spectral-line-intensity coefficients have been evaluated assuming equal populations of the four charge states providing the dominant contributions. The underlined transitions provide the dominant contributions to particular blended features.

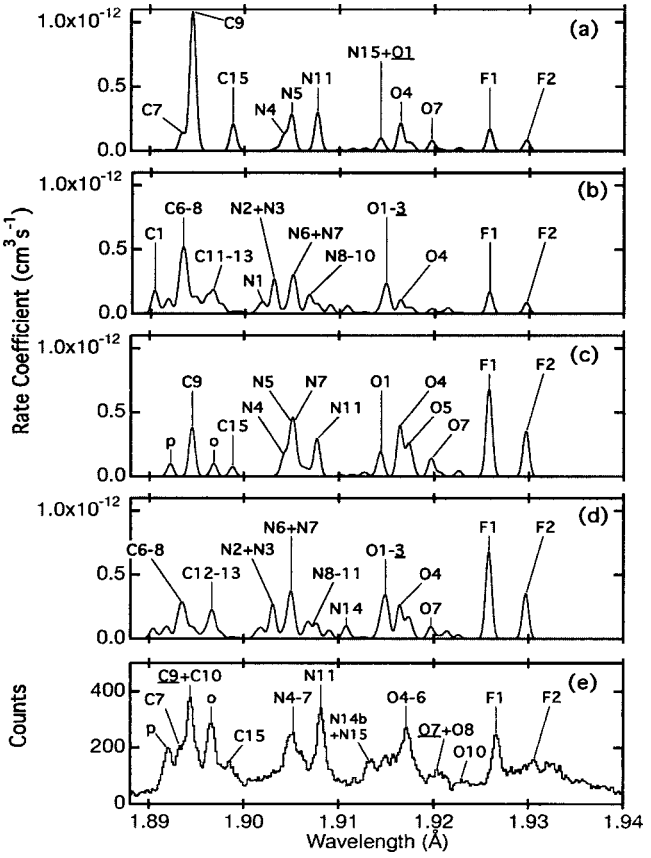

FIG. 3. $K\alpha$ emission spectra from Fe XVIII–Fe XXI, in the wavelength range 1.89–1.94 Å. The theoretically predicted spectral results are given for the contributions from collisional excitation in (a) the low-density and (b) intermediate-density regimes and from *K*-shell ionization in the (c) low-density and (d) intermediate-density regimes. The spectral-line-intensity coefficients have been been calculated assuming equal populations for the four charge states contributing to these spectra. The observed *K*-shell spectra of iron in the region 1.885–1.94 Å (e) have been measured on the EBIT-II under transient-ionization conditions at a beam energy of 12 keV. The experimental results are the first five, 7-ms duration, spectra recorded after the injection of iron into the trap. The underlined transitions provide the dominant contributions to particular blended features.

dicted using the actual monoenergetic distribution pertaining to our electron-beam observations, which has been deliberately selected to be outside the region of the autoionizing resonances.) The results exhibited in Fig. 3 include the theoretically predicted contributions from collisional excitation for (a) the low-density regime and (b) the intermediate-density regime; the theoretically predicted contributions from *K*-shell ionization for (c) the low-density regime and (d) the intermediate-density regime; and (e) the LLNL EBIT-II observations. We have emphasized that, for the nonresonant electron energies that we have considered in the present investigation, the dielectronic-recombination mechanism cannot contribute to the production of the $K\alpha$-emission spectra observed on EBIT-II. The results presented in Fig. 2 provide confirmation of the anticipated conclusion that the dielectronic-recombination mechanism cannot contribute to the experimental $K\alpha$-emission spectrum obtained at the nonresonant electron energy.

In order to facilitate the analysis of the experimental data, we present in Table I a tabulation of the intensities of the $K\alpha$ line emissions produced by collisional excitation and *K*-shell ionization for the two characteristic electron-density regimes used in our theoretical model and for three electron-density values considered by Lemen *et al.* [20]. In Table I, we have indicated the line identifications, from the heliumlike resonance line *w* to line $F2$ in Fe XVIII, as well as the corresponding experimental wavelengths. The detailed spectroscopic specifications of these lines, including the electronic-configuration assignments and angular-momentum couplings, have been tabulated by Beiersdorfer *et al.* [24]. The tabulated line intensities in Table I correspond to the following contributions: (a) collisional excitation predicted using our model for the low- and intermediate-density regimes (indicated by $I^{\rm exc}_{\rm low}$ and $I^{\rm exc}_{\rm intermediate}$, respectively), (b) collisional excitation predicted by the calculations of Lemen *et al.* [20] for the three density values considered, which are 10^{11}, 10^{13}, and 10^{15} cm^{-3} (indicated by $I^{\rm Lemen}_{11}$, $I^{\rm Lemen}_{13}$, and $I^{\rm Lemen}_{15}$, respectively), and (c) *K*-shell ionization predicted using cross sections derived from Lotz [18] and branching ratios taken from Jacobs *et al.* [14], for the low- and intermediate-density regimes (indicated by $I^{\rm ion}_{\rm low}$ and $I^{\rm ion}_{\rm intermediate}$, respectively). Note that, for all intensity ratios shown in Table I, equal population densities have been assumed for all charge states considered. This procedure allows radiative-emission models to be developed simply by multiplication with the charge-

TABLE I. Theoretically predicted relative line intensities for the spectral features observed in the $K\alpha$ emission spectrum of iron ions. $I^{\mathrm{exc}}_{\mathrm{low}}$ and $I^{\mathrm{exc}}_{\mathrm{intermediate}}$ denote the relative intensities for collisional excitation, by an electron beam with an energy of 12 keV, at low and intermediate electron densities, respectively. These line intensities have been calculated in the present investigation using the $K\alpha$ spectral model of Jacobs *et al.* [14,15]. The relative intensities denoted by I^{Lemen}_{11}, I^{Lemen}_{13}, and I^{Lemen}_{15} correspond to the relative collisional-excitation factors defined by Lemen *et al.* [20], for electron densities of 10^{11}, 10^{13}, and 10^{15} cm^{-3}, respectively, and obtained assuming a Maxwellian electron-energy distribution. These relative intensities have been calculated for the $K\alpha$ spectral lines in Fe XXII–Fe XIX. The intensities for collisional excitation, in each case, have been normalized relative to that of the strongest line in Fe XXII–Fe XIX. $I^{\mathrm{ion}}_{\mathrm{low}}$ and $I^{\mathrm{ion}}_{\mathrm{intermediate}}$ denote the relative intensities for *K*-shell ionization at low and intermediate electron densities, respectively, calculated (in the present work) using ionization cross sections from Lotz [18] and radiative branching ratios from Jacobs *et al.* [14,15].

Label	λ_{expt} (Å)	$I^{\mathrm{exc}}_{\mathrm{low}}$	$I^{\mathrm{exc}}_{\mathrm{intermediate}}$	I^{Lemen}_{11}	I^{Lemen}_{13}	I^{Lemen}_{15}	$I^{\mathrm{ion}}_{\mathrm{low}}$	$I^{\mathrm{ion}}_{\mathrm{intermediate}}$
w	1.850 40						0.0	48.8
x	1.855 32						0.0	81.3
t	1.857 08	38.5	47.6				0.0	25.4
y	1.859 53						0.0	48.8
q	1.861 01	242.0	299.1				0.0	66.9
r	1.863 72	67.0	82.7				0.0	18.8
z	1.868 15						100.0	48.8
*E*3 (β)	1.870 41	288.6	356.7				0.0	61.7
u	1.873 83	7.4	9.2				0.0	40.2
v	1.874 78	1.1	1.3				0.0	20.3
*E*16		6.2	7.7				23.7	15.4
	1.879 26							
*B*2		0.4	16.1	0.4	4.0	17.3	0.0	34.6
*B*3		3.8	100.0	4.0	24.7	100.0	0.0	16.0
*B*4	1.882 47	92.1	47.3	100.0	100.0	58.2	0.0	14.0
*B*5		80.6	37.3	93.4	92.5	50.4	0.0	21.0
*B*6		0.0	27.1	0.1	6.2	29.0	0.0	16.9
*B*7		21.8	11.2	23.4	23.3	13.6	0.0	3.3
	1.886 64							
*B*8		9.1	4.2	11.3	11.2	6.1	0.0	2.3
*C*1		0.0	19.7	0.0	1.1	13.4	0.0	11.0
*B*9		0.0	1.3	0.0	0.0	0.0	0.0	8.0
*B*10		0.8	0.4	0.0	0.0	0.0	20.6	2.7
p	1.892 06	0.1[a]					7.4	1.1
*C*4		0.0	2.4	0.0	0.0	0.0	0.0	3.8
*C*5		0.1	12.4	0.7	10.8	12.6	0.0	12.7
*C*6		0.0	23.4	1.2	19.5	25.0	0.0	19.1
	1.893 39							
*C*7		13.1	24.7	12.4	28.3	29.7	0.0	12.7
*C*8		0.0	30.6	0.0	4.6	44.3	0.0	25.6
*C*9	1.894 50	100.0	10.2	98.3	45.5	14.5	28.8	11.2
*C*10		5.5	10.4	5.0	11.4	12.0	0.0	5.4
*C*11		0.0	13.4	0.0	0.8	9.0	0.0	7.6
o		0.1[a]					7.5	1.1
	1.896 64							
*C*12		0.0	10.6	0.3	10.1	12.7	0.0	17.1
*C*13		0.0	11.5	0.5	8.2	10.9	0.0	18.8
*C*14	1.897 71	0.0	7.9	0.4	6.1	7.8	0.0	6.5
*C*15	1.898 62	19.3	2.0	20.5	9.5	3.0	5.6	2.2
*C*17	1.901 00	0.0	3.9	0.2	3.2	4.3	0.0	6.3
*N*1	1.902 30	0.0	8.0	0.0	1.1	6.8	0.0	9.4
*N*2		0.3	19.9	0.5	4.9	15.9	0.0	25.1
*N*3	1.903 55	0.0	10.8	0.0	0.3	6.6	0.0	13.6
*C*20		1.6	0.2	0.0	0.0	0.0	0.5	0.2
*N*4		11.4	3.1	11.0	10.4	4.7	8.3	6.5
	1.904 77							

TABLE I. (*Continued*).

Label	λ_{expt} (Å)	I_{low}^{exc}	$I_{intermediate}^{exc}$	I_{11}^{Lemen}	I_{13}^{Lemen}	I_{15}^{Lemen}	I_{low}^{ion}	$I_{intermediate}^{ion}$
*N*5		25.7	7.2	25.9	24.6	11.3	17.0	13.3
*N*6		0.2	15.0	0.2	3.7	12.0	0.0	31.8
	1.905 86							
*N*7		0.5	19.1	0.8	5.1	18.7	21.4	16.7
*N*8		0.1	6.3	0.2	1.6	5.2	0.0	7.9
*N*9	1.906 34	0.1	3.3	0.0	0.0	0.0	3.7	2.9
*N*10		0.0	8.3	0.0	1.1	7.1	0.0	9.7
*N*11	1.908 24	28.0	8.2	26.1	24.9	11.8	22.3	17.4
*N*12		0.1	5.7	0.1	1.4	4.6	0.0	7.3
	1.909 46							
*N*13		0.0	2.2	0.0	0.0	0.0	0.0	2.5
*N*13*a*		1.0	0.3	0.0	0.0	0.0	0.7	0.5
	1.910 81							
*N*14		0.1	7.0	0.1	1.8	5.6	0.0	14.5
*N*14*a*	1.911 63	1.0	0.5	1.9	1.8	0.8	1.1	0.9
*N*14*b*		2.0	0.6	2.4	2.3	1.1	1.6	1.3
	1.913 12							
*N*15		2.6	0.8	2.7	2.6	1.2	2.1	1.6
*O*1		7.1	6.6	11.1	11.8	8.9	13.0	16.9
*O*2	1.914 89	0.0	3.7	0.0	1.2	4.5	0.0	11.3
*O*3		0.5	23.0	0.6	3.2	20.7	0.0	38.2
*O*4		20.1	12.4	20.6	22.1	16.6	29.6	38.5
*O*5	1.917 33	4.4	4.1	6.8	7.3	5.4	16.4	21.3
*O*6		2.8	2.6	4.2	4.5	3.3	5.1	6.7
*O*7		7.4	4.6	7.7	8.3	6.2	10.7	13.9
	1.920 46							
*O*8		1.3	1.2	0.0	0.0	0.0	2.3	3.0
*O*9	1.921 27	0.1	5.3	0.1	0.7	4.8	0.0	8.7
*O*10	1.922 90	2.3	1.4	2.6	2.8	2.1	3.3	4.3
*F*1	1.926 79	15.7	19.6				51.3	100.0
*F*2	1.930 70	7.8	9.8				25.6	50.0

[a]The theoretical intensity values, at low electron density, for the lines *o* and *p* have been calculated using the HULLAC [19] by Osterheld [28].

balance fractions appropriate for different plasma conditions. Table I shows overall good agreement between the results of our collisional-excitation calculations for low densities and the theoretical predictions of Lemen *et al.* [20] that are presented for $N_e = 10^{11}$ cm^{-3}. We note that good agreement can also be found between our intermediate-density results and the predictions of Lemen *et al.* [20] for $N_e = 10^{15}$ cm^{-3}. Since the predictions of Lemen *et al.* [20] were obtained using a Maxwellian electron-energy distribution, precise agreement with the nonequilibrium predictions of our spectral model cannot be expected.

A. Collisional excitation and electron-density effects

For collisional excitation, the spectral-model predictions presented in Fig. 3, together with the tabulation of the spectral lines in Table I, illustrate the complexity of the radiative-emission spectra that are produced by the very large number of individual fine-structure lines occurring within the wavelength range 1.89–1.94 Å. We emphasize that only the most intense emission lines are listed in Table I. The combination of many additional emission lines, even with individual intensities that are relatively small, can provide substantial contributions to the observed emission spectra. These additional lines not only can produce substantial enhancements in the background of the measured spectra but also can provide significant effective (blended) contributions to the intensities of the more prominent lines [24]. These effects substantially complicate the interpretation of the observed spectral data.

The electron-density sensitivity of the $K\alpha$ radiative-emission spectra, which has been discussed in Sec. II, is primarily the result of collisional transitions among the fine-structure states of the ground-state electronic configurations. The electron-density dependence of the $K\alpha$ spectra is illustrated in Fig. 4, where we present theoretical predictions by Lemen *et al.* [20] for the $K\alpha$ emission spectra from Fe XIX–Fe XXI. In their calculations, account was taken of only the collisional-excitation mechanism, assuming a Maxwellian electron-energy distribution. Figure 4 shows the $K\alpha$ emission spectra obtained for two electron densities; (a) 10^{11} cm^{-3}, and (b) 10^{13} cm^{-3}. From the comparison of the results presented in Fig. 4 with our experimental spectral data, which are presented in Fig. 3(e), we find that the low-density (10^{11} cm^{-3}) spectra predicted by Lemen *et al.* [20] resemble more closely the experimental data than their

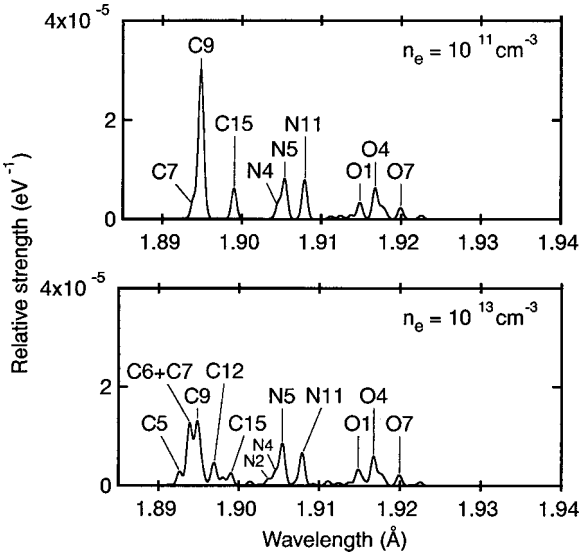

FIG. 4. Theoretically predicted spectra for collisional-excitation contributions adapted from Lemen *et al.* [20], including the contributions from Fe XIX–Fe XXI obtained for the two different electron densities (a) 10^{11} cm^{-3} and (b) 10^{13} cm^{-3}, and assuming a Maxwellian electron-energy distribution.

intermediate-density (10^{13} cm^{-3}) results. Similarly, the theoretical predictions of our low-density-regime spectral model, which are shown Fig. 3(a), resemble the experimental data more closely than the results obtained from our intermediate-density-regime model. Because of the assumption of a Maxwellian electron-energy distribution, the theoretical predictions of Lemen *et al.* [20] cannot be precisely compared with our EBIT-II experimental results, which are due to a highly nonequilibrium electron-energy distribution.

In astrophysical environments for which plasma-density effects could play an important role, such as stellar flares, prominent spectral features have been observed which can be used as diagnostics of the electron density in the wavelength range from 1.84 to 1.94 Å. The electron-density variation is found to be most pronounced for the line $C9$ in Fe XXI. The intensity of this spectral line decreases dramatically as the electron density increases. In the $K\alpha$ emission spectrum observed on EBIT-II, the spectral line $C9$ is blended with the lines $C8$ and $C10$, which are substantially enhanced with increasing electron density. However, the overall intensity of this spectral complex is diminished by a factor of 2 during the increase of the electron density from 10^{11} to 10^{13} cm^{-3}. Consequently, this spectral complex, which is centered at a wavelength of 1.894 50 Å, appears to present the best candidate for an electron-density diagnostic in the wavelength range from 1.84 to 1.94 Å.

B. *K*-shell ionization

In comparison with the spectra emitted from the most highly ionized Fe ions, which occur in the shorter-wavelength range 1.85–1.89 Å, much more complex spectra are emitted from the charge states from Fe XVIII through Fe XXI. For these ions, all significant spectral features that can be attributed to inner-shell ionization can also be generated by collisional excitation. Consequently, we find similarities between the collisional-excitation emission spectra shown in Figs. 3(a) and 3(b) and the *K*-shell ionization-produced emission spectra shown in Figs. 3(c) and 3(d).

Because of these similarities, we have not been able to identify any unambiguous *K*-shell ionization indicators for the charge states Fe XVIII–Fe XXI. However, the quantitative results presented in Table I can be used to determine the $K\alpha$-emission intensity ratios produced by resolved spectral features. By means of this procedure, the relative contributions of the various competing line-formation processes can be assessed. We have adopted a tentative charge-state-distribution model, in which all charge states have been assumed to have equal populations. A more detailed description, in which the charge-state distribution is more precisely determined from the individual ionization and recombination rates, is expected to be required for the accurate analysis of the emission-line intensity ratios produced by a combination of collisional excitation and *K*-shell ionization processes, which originate from different charge states. We also note that, since the final state of an ion after *K*-shell ionization corresponds to a ground or excited state in the next higher charge state (in which a single $1s$ electron has been removed), inner-shell ionization is particularly sensitive to the ground-state distribution and therefore to the electron density. This can be seen from a comparison of the low-and intermediate-density theoretical-simulation results presented in Table I, which shows significant differences between the two cases.

The spectral lines $C9$, $N7$, $N11$, $O4$, $F1$, and $F2$ have relatively large *K*-shell ionization contributions. Accordingly, these lines can be used as indicators of the *K*-shell ionization process. In addition, the observation of the two Fe XVIII spectral features $F1$ and $F2$ could be a sufficient indication of the presence of *K*-shell ionization. This is a consequence of their significantly large *K*-shell ionization rate coefficients and their relatively small collisional-excitation contributions (see Table I). Furthermore, the *K*-shell ionization contributions of these two Fe XVIII spectral features are further intensified as a result of the enhanced relative population of the closed-shell neonlike charge state Fe XVII.

C. Dielectronic recombination

The dielectronic-recombination satellite lines in Fe XXIII, and especially the satellite features k and j in Fe XXIV, had been considered to be the most useful diagnostics of the dielectronic-recombination process. However, these two charge states may not be sufficiently abundant under extreme nonequilibrium ionization conditions, which can occur in young supernova remnants. Accordingly, we have directed our attention to the less-frequently investigated dielectronic-recombination satellite lines in Fe XVIII–Fe XXI. From a comparison of the theoretically predicted dielectronic-recombination spectra, shown in Fig. 2, with the corresponding contributions from collisional excitation, indicated in Figs. 3(a) and 3(b), or from *K*-shell ionization, displayed in Figs. 3(c) and 3(d), significant differences are identified in the radiative-emission spectra, especially in the case

of Fe XXI. In contrast with the spectra arising from Fe XXIII and Fe XXIV (and as a consequence of the parity selection rules governing the transitions in these two ions), all dielectronic-recombination satellite lines in Fe XVIII–Fe XXI also acquire a collisional-excitation component (and often also a *K*-shell ionization contribution). Nevertheless, we have been able to identify useful indicators of dielectronic recombination in the Fe XXI complex. Here the blend consisting of the individual lines $C12$ and $C13$, with a wavelength centered at 1.896 64 Å, provides the dominant contribution to the dielectronic-recombination emission. We note that this $K\alpha$-emission feature cannot be excited by the other two line-formation mechanisms. Unlike the predictions for collisonal excitation and *K*-shell ionization, the use of a Maxwellian electron-energy distribution has been necessary in order to obtain the nonvanishing predictions for dielectronic recombination presented in Fig. 2. From a comparison of the theoretically predicted dielectronic-recombination spectra with our experimental results, it is found that the blended $C12/C13$ structure is absent from our EBIT-II data. This provides a further confirmation that the dielectronic-recombination mechanism cannot contribute in our experiment, as expected from our selection of the electron-beam energy sufficiently distant from any autoionizing resonance.

V. CONCLUSION

We have presented a detailed and systematic spectral model for the theoretical prediction of the $K\alpha$ x-ray emission from highly charged iron ions, in the wavelength range from 1.84 to 1.94 Å. Account has been taken of the fundamental radiative-emission processes associated with inner-shell electron collisional excitation, inner-shell electron collisional ionization, as well as dielectronic recombination. Particular emphasis has been directed at the identification of spectral features that can serve as diagnostics of extreme nonequilibrium or transient-ionization conditions, which can be encountered in stellar flares and supernova remnants, as well as tokamak plasmas. In order to provide a quantitative investigation of the dominant fundamental $K\alpha$ line-formation processes under these extreme nonequilibrium, transient-ionization conditions, we have employed our spectral model to make theoretical predictions for the $K\alpha$ x-ray emission spectra observed from Fe ions in the EBIT-II. We have considered all spectral features that can serve as diagnostics of the electron density, the line-formation mechanism, and the charge-state distribution. We have found that the observed spectroscopic features are well represented by the results of our theoretical predictions, providing an extension of earlier work on transient ionization [20].

In order to substantiate our theoretical predictions, we have presented high-resolution measurements of the $K\alpha$ radiative emission produced by highly charged Fe ions, from Fe XVIII to Fe XXV, under well-controlled and well-diagnosed laboratory conditions in a low-density environment. These measurements have been made using a transient-ionization technique that simulates extreme nonequilibrium conditions, which are believed to exist in astrophysical plasmas. Spectral signatures of the fundamental line-formation mechanisms have been identified. The identifications have been facilitated by utilizing the spectral predictions of atomic-physics models that have been developed for the description of the more complex atomic processes involving the intermediate charge states from Fe XVIII–Fe XXI. We have demonstrated that these spectral predictions are in good agreement with the experimental observations. While several useful diagnostic lines have been identified in the emission spectra from Fe XXII–Fe XXV, a more complex problem has been encountered for the other charge states below Fe XXII. Nevertheless, we have been able to employ our spectral model to produce reliable simulations of our experimental observations. We believe that this detailed spectroscopic model can provide substantial diagnostic capability, particularly for the determination of the basic physical properties of laboratory and astrophysical plasmas under extreme nonequilibrium ionization conditions.

In a future extension of this investigation, we plan to develop a more sophisticated spectral description for the theoretical prediction of the $K\alpha$ radiative emission. In the calculation of the collisional-excitation cross sections for the fundamental inner-shell-electron transitions, it would certainly be desirable to employ a more sophisticated calculation, which could be based on either the distorted-wave or close-coupling methods. However, we have emphasized that the incorporation of these more elaborate calculations for collisional-excitation processes alone would not necessarily provide a consistent improvement in the overall spectral description. The fundamental difficulty is that, for nonequilibrium ionization conditions, a more important contribution can arise from the collisional-ionization processes, for which cross-section calculations of comparable sophistication are not available for complex, many-electron atomic systems. Even the most recent advances in theoretical methods for the electron-impact ionization of simple, few-electron atomic systems have not overcome the well-known problem of three-body breakup in quantum mechanics, as discussed by Scott *et al.* [27]. Nevertheless, we plan to substantially extend the present spectral model by means of the incorporation of an explicit density-dependent (collisional-radiative) calculation of the excited-level populations (utilizing distorted-wave collision cross sections), the inclusion of additional contributions from higher-lying autoionizing states corresponding to outer-electron principal quantum numbers $n>2$, and a treatment of the polarized radiative emission that is produced by the directed-electron excitation processes in the EBIT-II experiments.

ACKNOWLEDGMENTS

This work has been supported by NASA Space Astrophysics Research and Analysis grants to LLNL and Columbia University, and performed under the auspices of the U.S. Department of Energy by the University of California Lawrence Livermore National Laboratory, under Contract No. W-7405-ENG-48. The work of V.L.J. has been supported by the U.S. Department of Energy, through Interagency Agreement No. DE-AI02-93-ER-54198 with the Naval Research Laboratory, and by the Office of Naval Research.

[1] H. Itoh, Publ. Astron. Soc. Jpn. **29**, 813 (1977).
[2] H. Itoh, Publ. Astron. Soc. Jpn. **30**, 489 (1978).
[3] P. R. Shapiro and R. T. Moore, Astrophys. J. **207**, 460 (1976).
[4] M. C. Kafatos and W. H. Tucker, Astrophys. J. **175**, 837 (1972).
[5] R. Mewe and J. Schrijver, Astrophys. Space Sci. **88**, 345 (1975).
[6] R. Mewe and J. Schrijver, Astron. Astrophys. **65**, 115 (1978).
[7] R. Mewe and J. Schrijver, Astron. Astrophys. **87**, 261 (1980).
[8] P. R. Shapiro and J. W. Knight, Astrophys. J. **224**, 1028 (1978).
[9] P. R. Shapiro and R. T. Moore, Astrophys. J. **217**, 621 (1977).
[10] P. Beiersdorfer, G. V. Brown, J. Crespo López-Urrutia, V. Decaux, S. R. Elliott, D. W. Savin, A. J. Smith, G. S. Stefanelli, K. Widmann, and K. L. Wong, Hyperfine Interact. **99**, 203 (1996).
[11] V. Decaux and P. Beiersdorfer, Phys. Scr., T **T47**, 80 (1993).
[12] V. Decaux, P. Beiersdorfer, A. Osterheld, M. Chen, and S. M. Kahn, Astrophys. J. **443**, 464 (1995).
[13] V. Decaux, P. Beiersdorfer, S. M. Kahn, and V. L. Jacobs, Astrophys. J. **482**, 1076 (1997).
[14] V. L. Jacobs, G. A. Doschek, J. F. Seely, and R. D. Cowan, Phys. Rev. A **39**, 2411 (1989).
[15] V. L. Jacobs, V. Decaux, and P. Beiersdorfer, J. Quant. Spectrosc. Radiat. Transf. **58**, 654 (1997).
[16] P. Beiersdorfer, R. Cauble, S. Chantrenne, M. Chen, N. DelGrande, D. Knapp, R. Marrs, A. Osterheld, K. Reed, M. Schneider, J. Scofield, B. Wargelin, K. Wong, D. Vogel, and R. Zasadzinsky, in *UV and X-Ray Spectroscopy of Astrophysical and Laboratory Plasmas*, edited by E. H. Silver and S. M. Kahn (Cambridge University Press, Cambridge, 1993), Vol. 59.
[17] M. J. Seaton, Adv. At. Mol. Phys. **11**, 83 (1975).
[18] W. Lotz, Z. Phys. **216**, 241 (1968).
[19] A. Bar-Shalom, M. Klapisch, and J. Oreg, Phys. Rev. A **38**, 1773 (1988).
[20] J. R. Lemen, K. J. H. Phillips, R. D. Cowan, J. Hata, and I. P. Grant, Astron. Astrophys. **135**, 313 (1984).
[21] M. A. Levine, R. E. Marrs, J. R. Henderson, D. A. Knapp, and M. B. Schneider, Phys. Scr., T **T22**, 157 (1988).
[22] R. E. Marrs, M. A. Levine, D. A. Knapp, and J. R. Henderson, Phys. Rev. Lett. **60**, 1715 (1988).
[23] L. von Hámos, Ann. Phys. (Leipzig) **17**, 716 (1933).
[24] P. Beiersdorfer, T. Phillips, V. L. Jacobs, K. W. Hill, M. Bitter, S. von Goeler, and S. M. Kahn, Astrophys. J. **409**, 846 (1993).
[25] I. G. Brown, J. E. Galvin, R. A. McGill, and R. T. Wright, Appl. Phys. Lett. **49**, 1019 (1986).
[26] B. M. Penetrante, M. A. Levine, and J. N. Bardsley, in *International Symposium on Electron Beam Ion Sources and Their Applications*, edited by Ady Hershcovitch, AIP Conf. Proc. No. 188 (AIP, New York, 1989), p. 145.
[27] M. P. Scott, T. Stitt, N. S. Scott, and P. G. Burke, J. Phys. B **35**, L323 (2002).
[28] A. L. Osterheld (private communication).